Radiation Physics and Chemistry 181 (2021) 109335

Contents lists available at ScienceDirect

Radiation Physics and Chemistry

journal homepage: www.elsevier.com/locate/radphyschem

The response of low-cost photodiodes for dosimetry in electron beam processing

Josemary A.C. Gonçalves [a], Alessio Mangiarotti [b], Viviane K. Asfora [c], Helen J. Khoury [c], Carmen C. Bueno [a,*]

[a] Instituto de Pesquisas Energéticas e Nucleares, 05508-000, Cidade Universitária, São Paulo, Brazil
[b] Instituto de Física, Universidade de São Paulo, 05508-080, Cidade Universitária, São Paulo, Brazil
[c] Departamento de Energia Nuclear, Universidade Federal de Pernambuco, Recife, PE, 50740-545, Brazil

ARTICLE INFO

Keywords:
Radiation processing dosimetry
Si PIN Photodiode dosimeter
Electron dosimetry

ABSTRACT

The response of thin diodes (SFH206k) as dosimeters has been investigated employing the beam of an electron accelerator within the dose rate range of 2–8 kGy/s and accumulated doses up to 100 kGy. These devices, operating in the short-circuit mode and under industrial irradiation conditions, deliver current signals non-linearly dependent on the dose rate, whichever the dose history of the diodes, due to the high density of the generated electron-hole pairs herein achieved. Despite this nonlinearity, the dose rate response is stable and characterized by current signals with repeatability better than 2.0%, regardless of the accumulated dose. It is also found that the dose responses are quite linear with sensitivities slightly dependent on the accumulated dose at a constant dose rate. The decrease in the charge sensitivity, taking as reference that obtained before any radiation damage, reaches only 9% (k = 2) at 100 kGy, which is much smaller than the values reported in the literature. From this low aging and the repeatability of both dose rate and dose responses, it seems that the photodiode under investigation is a low budget alternative, good enough for routine dosimetry, provided it has been previously calibrated in the same processing facility.

1. Introduction

Electron beam (EB) processing uses energetic electrons from particle accelerators to irradiate products to preserve or modify their characteristics. The key advantage of this technique relies on achieving reproducible chemical and biological effects on the material by controlling the delivery of known absorbed doses of radiation. Currently, the sterilization of medical devices, the treatment of foodstuffs, and the modification of polymers are the main applications for industrial radiation processing (Cleland, 2006; Calvo et al., 2012). This broad range of activities requires accurate dosimeters for standardization as well as those less precise but useful for routine measurements or absorbed-dose mapping. In general, EB processing applications comprise high absorbed doses (10–100 kGy), ultra-high dose rates (kGy/s), and harsh environmental conditions, providing stringent dosimetric and regulatory requirements for dosimetry (ICRU Report 80, 2008). Several well-established high dose dosimetry systems, such as calorimeters, alanine, and polymers (polymethyl methacrylate, cellulose triacetate, radiochromic films) meet most of these requirements, being suitable for absolute and relative dose measurements at electron beam facilities (ISO/ASTM 52628, 2013; ISO/ASTM 51649, 2015). Nevertheless, since in almost all of these dosimeters the reading of the parameters is performed with some delay after the end of the irradiation, there is still interest in either devising new real-time devices or improving the performance of the existing ones. The most important motivation for using real-time dosimeters in electron processing stems from their capability to measure instantaneous dose rates, allowing them to continuously monitor drifts in the accelerator parameters. Such information is relevant to schedule the needed maintenances of the facilities, avoiding unexpected shutdowns, and the corresponding increases in production costs (Kneeland et al., 1999).

Real-time electronic dosimeters are generally based on diodes, transistors, and solid state ionization chambers made of silicon dioxide or diamond. They have been extensively applied for electron and photon dosimetry in radiation protection, medical imaging, and radiation therapy. A detailed description of these applications and the state of the

* Corresponding author. Av. Lineu Prestes 2242, Cidade Universitária, 05508-000, São Paulo, SP, Brazil.
E-mail address: ccbueno@ipen.br (C.C. Bueno).

https://doi.org/10.1016/j.radphyschem.2020.109335
Received 15 July 2020; Received in revised form 8 October 2020; Accepted 25 December 2020
Available online 1 January 2021

art in electronic dosimetry can be found in the articles published by Barthe (2001), Rosenfeld (2007), Damulira et al. (2019), and those referenced therein.

The use of electronic dosimeters for radiation processing purposes began in the mid-1970s. In general, the measurement of interest is the dose rate, which is correlated with the current generated in silicon devices, for either monitoring or mapping the steady-state fields of the gamma rays from high activity ^{60}Co sources. The first attempts made to employ diodes for the quantification of high doses were described in several articles available in the literature (Muller, 1970a, b; Osvay et al., 1975; Möhlmann, 1981; Dixon and Eckstrand, 1982). The majority of these authors reported the linearity between currents and dose rates within different ranges and the rapid aging of the diodes under prolonged gamma irradiation. Additionally, the quality inhomogeneity among the available diodes varied to a great extent, so different samples of the same type and batch presented distinct response characteristics. These systems required a sample-specific dosimetric calibration, which is impractical for routine dosimetry. Due to all these drawbacks, so far, silicon diodes are not listed in the dosimetry systems recommended for use in radiation processing (ICRU Report 80, 2008; ISO/ASTM 51649, 2015).

However, the physics underlying the aging of diodes has been extensively investigated in the framework of high energy physics experiments to develop silicon devices more resistant to the damage induced by photons, neutrons, and ionizing particles. For a review of these issues, the reader is referred to Moll (2018). From the available literature, it is well known that the key parameter to describe the decrease of the current sensitivity of the diode is the minority carrier diffusion length (Osvay and Tárczy, 1975; Casati et al., 2005; Bruzzi et al., 2007). It is proportional to the square root of the minority carrier lifetime, which in turn is inversely proportional to the defect concentration. When the diffusion length decreases below the thickness of the diode, its sensitivity starts to decrease drastically. Two experimental approaches are adopted to overcome this difficulty: i) to pre-irradiate the device to introduce by radiation-induced damage so many defects that the relative change of the diffusion length becomes negligible; ii) to select thin diodes with thicknesses smaller than the lowest minority carrier diffusion length anticipated at the foreseen accumulated dose. For high dose applications, the first strategy is not cost-effective and induces new parasitic properties, like, for example, significant temperature dependence and poor sensitivity (Barthe, 2001). The second strategy seems to be achievable with thin optical sensors, such as photodiodes, which feature low dark currents, high stability, and a very small temperature coefficient. Furthermore, the constantly improving industrial production of these devices warrants the high reproducibility of their electric parameters in large batches at a very low cost. In this context, the real-time response of a commercial thin photodiode (SFH206k) for gamma radiation processing applications was recently investigated focusing on the variation of the current sensitivity with accumulated doses up to 15 kGy (Gonçalves et al., 2020).

In the present work, the response of the same type of photodiode has been investigated for electron beam (EB) radiation processing with twofold goals: i) to confirm our previous findings regarding the stability of the current sensitivity, as well as the dose lifespan of the diode; ii) to broaden the field of application of the diode to absorbed doses lower than 25 kGy, typically reached in several applications for EB processing (Cleland, 2006; Calvo et al., 2012).

2. Materials and methods

Five photodiodes (SFH206k supplied by Osram®) with full wafer thickness of (230 ± 5) μm and 7.0 mm^2 sensitive area encapsulated into a plastic casing were used in this work. The batch uniformity was evaluated by measuring dark currents and capacitances as a function of the reverse voltage (0–30 V) at ambient temperature (23 °C). Typically, all devices exhibit very low dark currents, 0.17 nA (0 V) up to 1.46 nA (30 V), and capacitances from 72 pF (0 V) down to 10 pF (30 V). Variations in both current and capacitance measurements of the batch are found to be less than 5%. The dosimeter-to-dosimeter variability (3%) of these diodes has been evaluated by previously irradiating all diodes to 10 Gy in a ^{60}Co Panoramic irradiator of type II (Yoshizawa Kiko Co, Ltd). Such a small dose, which is negligible when compared to those herein achieved with the electron beam accelerator, is chosen to prevent the diodes from suffering any radiation damage.

To be used as dosimeters, each diode was placed in house-made polymethylmethacrylate (PMMA) cylindrical probe (9 mm in diameter and 45 mm length) provided with a miniature coaxial connector with a push-pull self-latching system (Lemo®). A 20 m coaxial cable connects the front p+-layer electrode of the diode to the input of a Keithley 6517B electrometer, configured as an amp-meter with the speed of one power line cycle, digital filter on, and range set at 200 μA. The conducting shield of the cable was employed to connect the back n+-layer to the ground of the electrometer. Before acquiring each series of data, an offset adjustment procedure (zero correct) was performed to minimize the input bias (offset) current to 5 nA and voltage burden less than 100μV, leading to an accuracy of (0.1% of reading +5 nA) for currents up to 200 μA. All current measurements were carried out in short-circuit mode, with the diode unbiased and its back layer (n^+) grounded. For analysis, the data acquired by the electrometer were directly sent to a personal computer via the GBIP interface controlled by a software developed in LabView.

The irradiations were performed at a facility (DC 1500/25/04 – JOB 188), maintained by the Instituto de Pesquisas Energéticas e Nucleares (IPEN-CNEN/SP), with a 1.5 MeV electron beam (EB), which was previously characterized by using alanine pellets read with an electron paramagnetic resonance (EPR) spectrometer, and cellulose triacetate (CTA) films read with a spectrophotometer. The relevant accelerator parameters are the following: electron energy (1.43 MeV), scan width of 1.02 m, spot size (beam length) of 2.54 cm, surface dose uniformity better than 6.2% (k = 2) in the center of the scan width. All these figures came from the dosimetric characterization of the electron beam in terms of its Operational Qualification according to ISO/ASTM 51649 (2015). More experimental details can be found in our previous article (Kuntz et al., 2015).

Irradiations were carried out with the probe positioned at 17 cm from the scan window and at the center of the scan width, where the surface dose is the most homogeneous. The dosimeter was placed on the top of a 2.0 cm thick wooden plank, which was settled down in the tray to prevent the diode from being irradiated by electrons backscattered on both the stainless steel conveyor and tray. To be irradiated, this assembly is sent through the radiation field in the conveyor direction with a speed of 6 m/min. The net temperature rise during the exposure is monitored by an irreversible temperature indicator (GEX, model P8003) placed side-by-side to the dosimetry probe. To help the reader, a schematic diagram of the experimental setup is shown in Fig. 1.

The dose rate response was investigated by measuring the radiation-induced current within the dose rate range of 2–8 kGy/s achieved by varying the beam current from 0.5 mA up to 2 mA. The corresponding doses received by the diodes in one pass through the irradiation zone at a constant speed (6 m/min) are shown in Table 1.

The repeatability of the dose rate response is given by the coefficient of variation CV (percentual ratio of the standard deviation to the average value of the peak current) of five current signals, consecutively recorded at the same dose rate during each transit of the diode through the radiation field. This procedure, which is recommended for clinical photon beam dosimetry (IEC 61674, 2012), was applied in this work due to the lack of protocols for diodes in radiation processing dosimetry.

The dose-response was extracted from the charge, assessed off-line through the integration of the current signals, as a function of the dose within the range of 1 kGy–25 kGy. The charge sensitivity, defined as the charge per unit of absorbed dose, is experimentally determined through the slope of the charge versus the absorbed dose plot. Unless

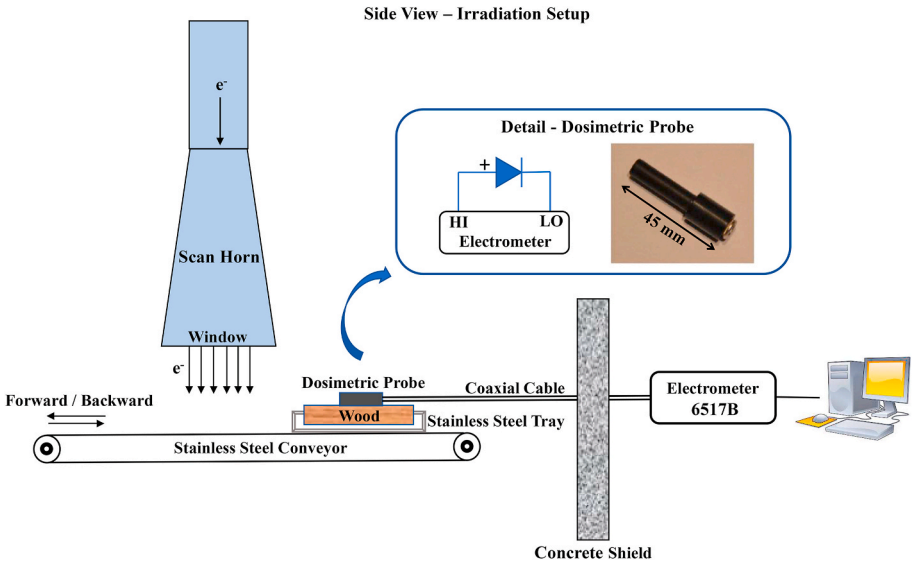

Fig. 1. Schematic diagram of the experimental setup.

Table 1
Doses received by the diodes in one pass through the irradiation zone at 6/min speed over a dose-rate range of 2–8 kGy/s.

Beam Current (mA)	Dose rate (kGy/s)	Dose per pass (kGy)
0.5	2	0.5
1.0	4	1.0
1.5	6	1.5
2.0	8	2.0

otherwise stated, all dose-response measurements were performed at 4.0 kGy/s dose rate and 6 m/min conveyor speed, corresponding to a dose of 1 kGy in one single pass of the diode through the irradiation zone. These features were chosen to replicate the real experimental conditions of most radiation processing applications conducted by this EB facility.

The experimental approach adopted to investigate the influence of the accumulated dose on the performance of the diode is to compare its dosimetric response before any radiation damage (hereafter identified as the *pristine diode* and used as a reference for 0 Gy) to those assessed after accumulating fractions of the dose of 25 kGy up to 100 kGy. In between each step of irradiation, measurements of dark currents versus reverse voltage were also performed aiming at monitoring the presence of radiation damage effects. The influence of the accumulated dose on the repeatability of the current signals was also evaluated following the same procedure described above. The combined standard uncertainties of the experimental results are obtained by adding all the components (types A and d B) of the standard uncertainties in quadrature (JCGM, 2008; ISO/ASTM 51707, 2015). The expanded uncertainties were calculated with a coverage factor k = 2 providing a confidence level of about 95%.

3. Results

3.1. Dose rate response

Five current signals delivered by a pristine diode, consecutively irradiated to different dose rates, are displayed in Fig. 2. All the signal profiles have great similarities and the expected increase in the peak current corresponding to higher dose rates is visible. The measurements of the repeatability of each set of signals, read out at the same dose rate, yield coefficients of variation in the peak currents smaller than 2.0% even at 2 kGy/s, which is the lowest dose rate attainable with the accelerator used in this work.

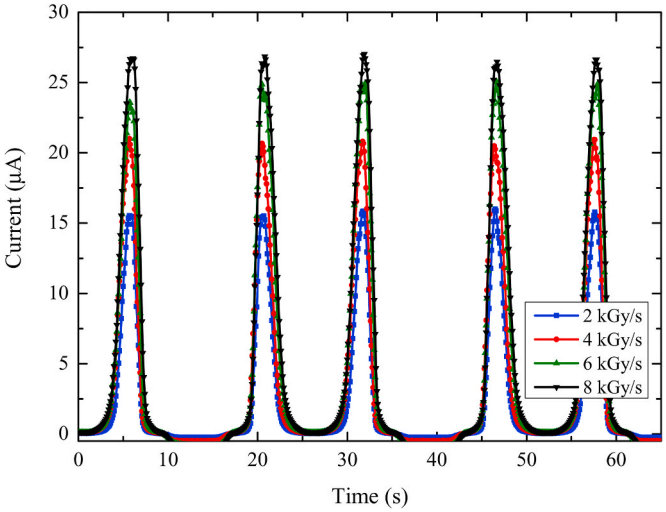

Fig. 2. Current signals delivered by the pristine diode irradiated at dose rates varying from 2 kGy/s to 8 kGy/s. Each signal corresponds to one single transit of the diode through the radiation field in the conveyor direction. Instrumental uncertainties of the current measurements are smaller than the size of the symbols.

The expanded view of one current signal measured at 4 kGy/s as a function of the distance traveled by the diode through the radiation field is depicted in Fig. 3. Two main features can be observed in this plot: the peak current is registered when the diode is positioned at the center of the scan window and, even when it is outside of this region, it remains rather sensitive to scattered electrons. Taking into account the time duration of the diode exposure corresponding to the peak region and the conveyor speed of 6 m/min, the maximum current is delivered over a traveling distance (the hatched region in Fig. 3) equal to the length (one inch) of the scan window. The full width at half maximum (FWHM) of the current signal is (18.8 ± 0.3) cm.

To check whether the signal profile is dependent on the conveyor speed, the current signals have been recorded at 4 kGy/s covering the speed range from 2 m/min to 6 m/min. As it can be seen in Fig. 4, the FWHM of the signals and the traveling distance corresponding to the peak currents delivered by the photodiode remain almost constant

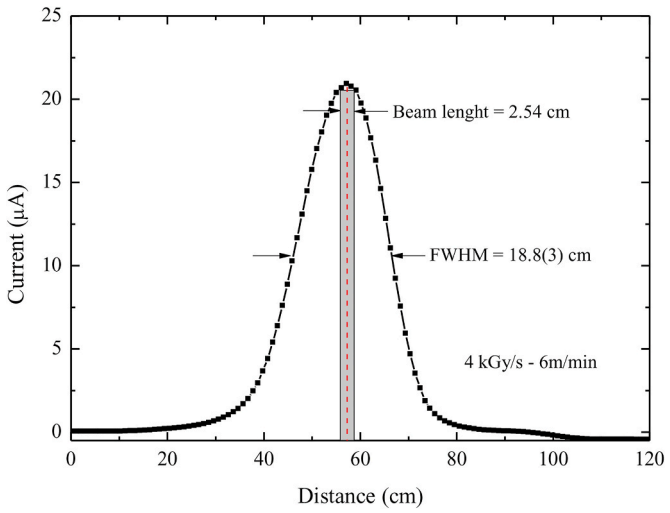

Fig. 3. Expanded view of a current signal recorded at 4 kGy/s while one pristine diode moves through the radiation field in the conveyor direction. The exposure time is converted to traveling distance taking into account the conveyor speed of 6 m/min. The length (one inch) of the scan window is hatched in the plot.

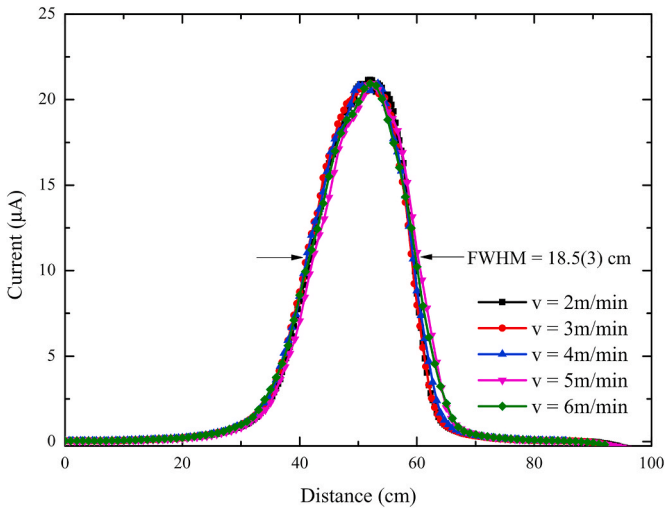

Fig. 4. Expanded view of the current signals delivered by one pristine diode irradiated at 4 kGy/s for different conveyor speeds ranging from 2 m/min to 6 m/min. The agreement among the FWHM values is better than 2%.

regardless of the conveyor speeds. The mean value of the FWHM is (18.5 ± 0.3) cm.

The dose rate response of the diode is shown in Fig. 5, where each value of the current is the average of the five peak current signals exhibited in Fig. 2. Within the range from 2 to 8 kGy/s, the peak currents increase, although not linearly, with the dose rate and tend to saturate for dose rates higher than 6 kGy/s. This behavior is also observed in the dose rate responses of the same diode after accumulating 50 kGy and 100 kGy, which are plotted in the same figure for comparison. The latter results also evidence the decrease of the current sensitivity, as well as the saturation of the peak current, with increasing dose rates. Theoretically, the non-linear dependence of the current on such high dose rates, even for the pristine diode, can be associated with the imbalance between the generation and recombination rates of the charge carriers. Then, in an attempt to give numerical support to explain these results, simulations and calculations (detailed in section 4) have been performed to assess the energy deposited by the electrons incident on the diode and the

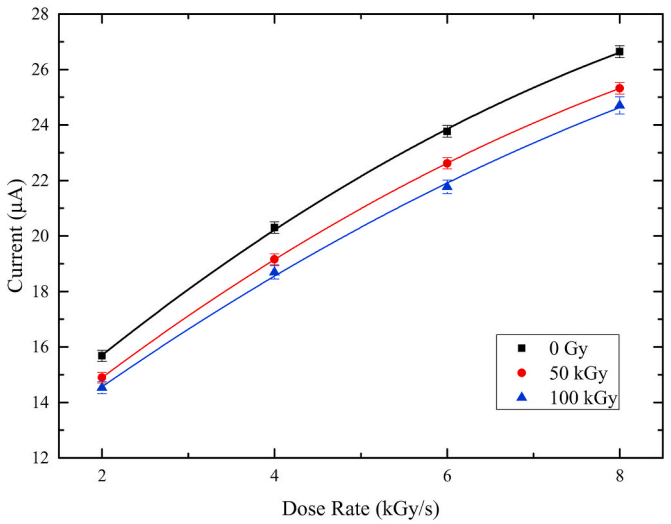

Fig. 5. Dose rate responses of one pristine diode (0 Gy) and after accumulating 50 kGy and 100 kGy. Each value of the peak current is the average of five current signals consecutively read out at the same dose rate.

corresponding electron-hole generation rates.

Despite the evident nonlinearity between peak currents and dose rates, the current signals, recorded at 4 kGy/s, are very reproducible as shown in Fig. 6. Indeed, the corresponding coefficients of variation in the peak current values are found to be 1.8% (0 Gy) and 1.2% (100 kGy), which are less than the expanded uncertainty (6.2%) of the calibration of the facility.

In the same figure, the effect of the accumulated dose on the decrease of the sensitivity is also evident. It is important to note that the background currents, measured before and after each transit of the diode through the radiation field with the beam on, remain almost constant (50 nA on average), whichever the accumulated dose. These small background currents lead to current-to-noise ratios of almost 400 even when the diode is irradiated up to 100 kGy.

3.2. *Dose-response*

The dose responses of the same diode, before any irradiation and

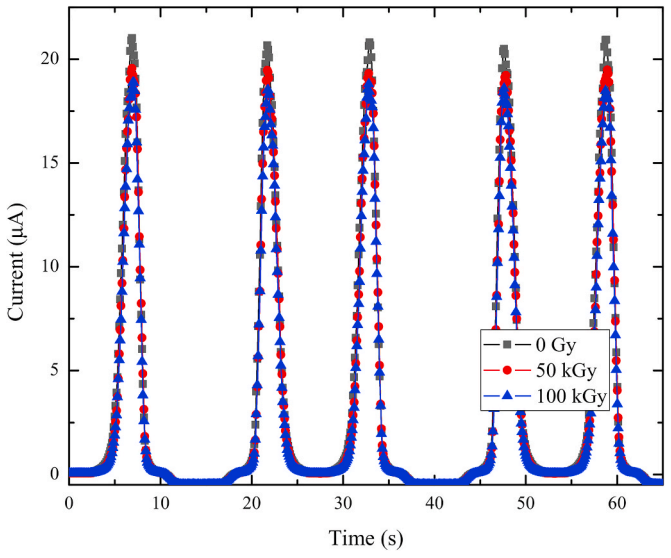

Fig. 6. Repeatability of five consecutive transits of the pristine diode (0 Gy) and after accumulating 50 kGy and 100 kGy. Irradiations have been performed with a dose rate of 4 kGy/s.

after being irradiated up to 100 kGy in steps of 25 kGy, are shown in Fig. 7.

It can be seen that all sets of data exhibit a similar linear pattern between the charge generated in the sensitive volume of the diode and the absorbed dose varying from 1 kGy to 25 kGy. However, the slope of each dose-response curve, which is a measure of the charge sensitivity (S_c), is slightly dependent on the accumulated dose. There is a visible decay trend of the charge sensitivity data with the accumulated dose (Table 2) reaching almost 9% at 100 kGy. To quantify this dependence, the ratio between the charge sensitivity attained after and before irradiation is plotted as a function of the accumulated dose in Fig. 8.

The data presented in Fig. 8 evidence the gradual and continuous decay of the charge sensitivity with increasing accumulated dose, reaching only 9% at 100 kGy. This decrease is much smaller than the typical loss in sensitivity (20–25% for doses $\geq$ 10 kGy) of commercial diodes operating without externally applied voltages (Osvay and Tárczy, 1975; Grusell and Rikner, 1984; Gilar and Petr, 1985; Rikner and Grussel, 1987; Barthe, 2001; Marre and Marinello, 2004). As previously stated, this low aging is expected to occur in an unbiased diode whose thickness is smaller than the minority carrier diffusion length at 100 kGy. To ascertain whether this assumption is correct or not, semi-empirical calculations are made in section 4 and discussed in section 5.

As the sensitivity decay is physically related to the onset of radiation damage effects, responsible for an increase in the dark current growth, this later parameter can be indirectly used to monitor the damage on the diode irradiated up to 100 kGy. For this purpose, measurements of dark currents (I) as a function of the reverse voltage (V) have been carried out shortly after the end of each step of irradiation up to 100 kGy. To ease visualization, only I–V curves of the pristine diode and irradiated to 50 kGy and 100 kGy are presented in Fig. 9.

As it can be seen in Fig. 9, all I–V curves exhibit similar shapes characterized by the increase of the dark current with reverse bias and accumulated dose. For example, the dark current varies from 0.17 nA (0 Gy) to 0.36 nA (100 kGy) at 0 V and from 1.46 nA (0 Gy) to 13.65 nA (100 kGy) at 30 V. As a matter of fact, at 0 V the dark current is about three orders of magnitude lower than that induced during the measurements by the beam, even when the diode is heavily irradiated to 100 kGy.

All these results confirm the double advantages of the lowest generation of dark currents and the smallest difference between the dark

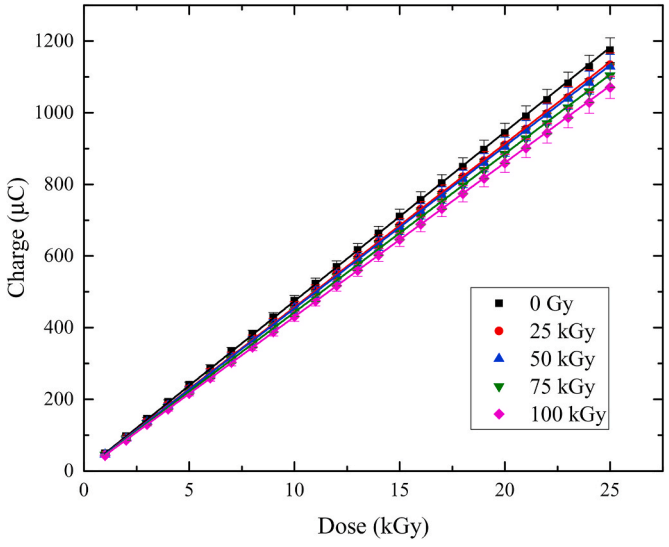

Fig. 7. Dose-response curves obtained with the same diode for initial doses of 0, 25, 50, 75, and 100 kGy. Each dose-response curve was measured over a 25 kGy dose range at incremental dose steps of 1 kGy.

Table 2
Charge Sensitivity (S_c) of the same diode before irradiation and after being irradiated up to 100 kGy in steps of 25 kGy. Standard errors are provided by the linear fitting of the datasets.

Accumulated Dose (kGy)	S_c (μC/kGy)
0	47.2 ± 0.8
25	45.6 ± 0.8
50	45.3 ± 0.8
75	44.3 ± 0.8
100	43.0 ± 0.8

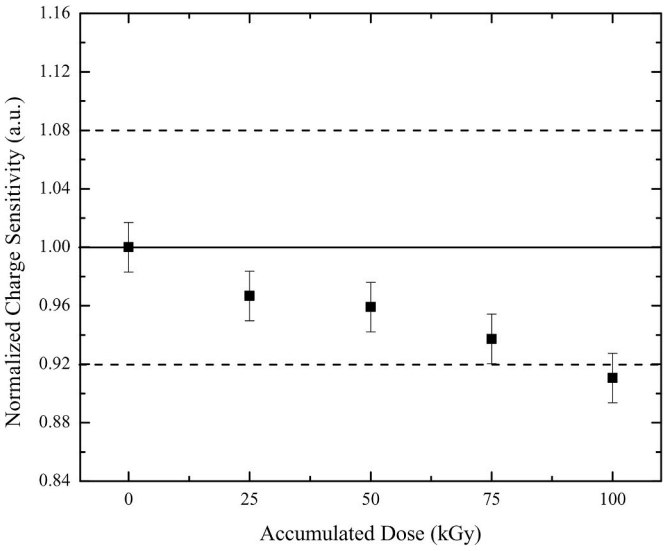

Fig. 8. Charge sensitivities of the same diode irradiated at different doses normalized to that attained before any irradiation (0 Gy) as a function of the accumulated dose. The dashed lines show the maximum allowed response variation (8%, k = 2) of routine dosimeters for EB processing according to ISO/ASTM 51649 (2015).

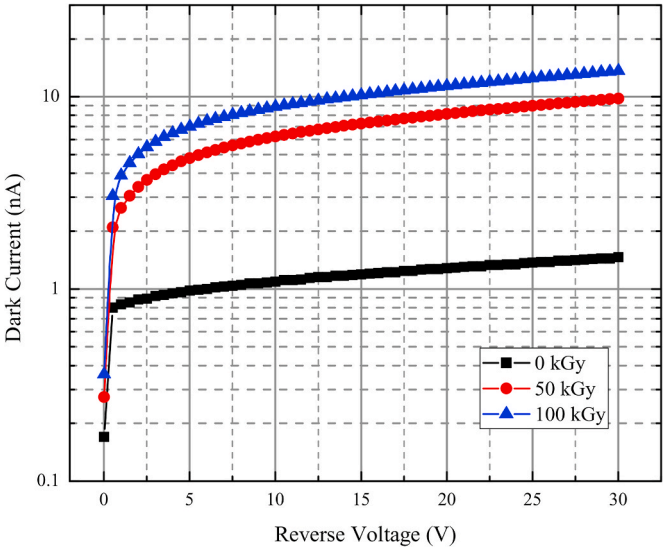

Fig. 9. Dark current as a function of the reverse voltage of one pristine diode (0 Gy) and after irradiation to 50 kGy and 100 kGy.

currents after and before radiation damage when using the diode without externally applied voltage.

4. Simulations and calculations

4.1. Energy deposited on the diode and electron-hole generation rate

In this work, the deposited energy has been assessed through simulations performed with the Monte Carlo code PENELOPE/pencyl version 2018 (Baró et al., 1995; Sempau et al., 1997; Salvat, 2019). This code is particularly suited to simulate electrons propagating in matter with energies of few MeV down to few keV, owing to the particular implementation of the transport mechanics of charged particles (Benedito et al., 2001), needed to properly describe the effect of multiple scattering, and the accurate modeling of elastic and inelastic scattering cross-sections. The elastic scattering cross-sections were calculated employing partial wave expansions in a mean central field obtained from a Dirac-Fock self-consistent procedure. The same values were also separately published in the ICRU Report 77 (Berger et al., 2007). Inelastic cross-sections were obtained in the Plane Wave Born Approximation with a Sternheimer-Liljequist Generalized Oscillator Strength model tuned to reproduce the average stopping powers from the ICRU Report 37 (Berger et al., 1984). Extensive benchmarking of the PENELOPE code was published by Benedito et al. (2001) and Sempau et al. (2003). These authors compared PENELOPE to experimental data on the fraction of backscattered electrons from thin metallic foils and their energy distribution and the transmitted fraction of electrons and their energy distribution.

In the present simulation, the volumes included are the titanium exit window of the beam, the air column, the entrance face of the probe, the entrance face of the plastic casing of the diode, the diode itself, the exit face of the casing, the exit face of the probe, and a polystyrene volume simulating the wooden plank supporting the setup. The main reason for not using wood in the simulations is the variability and complexity of its composition. Polystyrene, whose chemical composition is very well known, is a standard dummy material in EB processing with depth dose curves and practical range quite similar to wood (for 1.5 MeV electrons).

The thickness of the active volume of the diode is not enough to stop the electrons, even taking into account the presence of the other materials in front of it. Thus, energy loss fluctuations are expected to be important and materials on the exit path have to be included because they can backscatter electrons into the active volume. For the same reason, the initial horizontal position of the simulated beam has been smeared to illuminate the full face of the plastic probe. The simulation improves on a simple continuous slow-down approximation (CSDA) estimate because it takes into account electron multiple scattering, backscattering from volumes outside the active one, and energy loss straggling. The number of simulated primary electrons from the beam is $5 \cdot 10^6$, taking approximately 68 h on a modern computer with a 64-bit CPU running at 2.0 GHz (Opteron 6128 HE manufactured by AMD®). The tracking parameters C1 (limit on the average angular deflection per step), C2 (limit on the average fractional energy loss per step), Wcc (energy loss threshold in eV for hard inelastic collisions), and Wcr (energy loss threshold in eV for hard bremsstrahlung events) have all been set to zero resulting in a detailed simulation with absorption cuts set at 1 keV for electrons and positrons and at 0.1 keV for photons in all the materials included. The average energy deposited in the active volume of the diode is (164 ± 1) keV, where the indicated uncertainty represents one standard deviation obtained by propagating the statistical uncertainty of each channel of the energy deposition histogram given by PENELOPE/pencyl.

This result allows the generation rates to be roughly calculated, taking into account the energy (3.2 eV) needed to produce an electron-hole pair in silicon and the electron fluence rates ($1.2–4.9 \cdot 10^{13}$ e/cm^2.s) reaching the diode. From these calculations, it turns out that a huge number of 0.6–2.5 $\cdot 10^{19}$ electron-hole pairs is generated in one cubic centimeter per second. These values are almost three orders of magnitude bigger than the intrinsic silicon doping (10^{15}-10^{16}cm^{-3}) for ordinary diodes, commonly used in clinical photon/electron beam dosimetry (Rosenfeld, 2007). This comparison is equally valid for the SFH206k diode, despite the lack of information on its doping concentration, owing to the special features of the PIN structure. The one that matters most here is that the major contribution to the induced current is due to electron-hole pairs generated and collected in the intrinsic region, regardless of the diode being biased or not, due to the huge doping concentration of the P and N layers. So, for comparative purposes, it is acceptable to consider only the concentration of dopants in the intrinsic region of the photodiode.

4.2. Minority carriers diffusion length

It is well-known that the decrease in the excess minority carrier diffusion length with increasing accumulate dose is responsible for the drop in the sensitivity of unbiased diodes subjected to irradiation. As stated earlier (section 1), this sensitivity decay can be negligible in a diode with a thickness less than the minority carrier diffusion length anticipated at the foreseen accumulated dose. This condition might hold in this work, mainly based on the results presented in Figs. 7 and 8. The simplest way to check this hypothesis is to compare the minority carrier diffusion length at 100 kGy with the full thickness of the diode. However, to the best of our knowledge, this information is not available in the literature. In an attempt to add some numerical support to this analysis, the diffusion length (L) of the excess minority carrier is estimated using the equation $L = (D \cdot \tau)^{1/2}$, where D is the diffusion coefficient and τ the lifetime of the minority carrier (hole in n-type silicon). The first parameter is calculated taking into account the published values of intrinsic silicon doping and hole mobility at 300 K (Gildenblat et al., 1996). The lifetime is estimated from the dark current delivered by the pristine diode fully depleted and irradiated to 50 kGy and 100 kGy (Fig. 9), following the approach adopted by Kitaguchi et al. (1996). Despite using a single lifetime constant and the intrinsic silicon doping, which might be an oversimplification, the hole diffusion length is found to decrease from 790 μm to 259 μm with doses varying between 0 Gy and 100 kGy. Such values of the diffusion length are higher than the thickness of the diode (230 μm) and justify the proposed interpretation of the small decrease in the charge sensitivity with accumulated dose. Moreover, this is also an indirect confirmation that the diode, even when irradiated to 100 kGy, is indeed thin in comparison to the minority carrier diffusion lengths.

5. Discussion

The dose rate responses of either preirradiated or pristine diodes have revealed that the induced currents dependent nonlinearly on the dose rate within the range of 2–8 kGy/s. This saturation in the dose rate response can be partially explained by the Shockley-Read-Hall (SRH) theory (Schockley and Read, 1952; Hall, 1952), according to which the linearity between current and dose rate is only achieved if the recombination rate is proportional to the number density of excess minority carriers (Δn). This requirement is met when Δn is much smaller than the number density of the doping of the silicon base (N), i.e., for low doses rates. In this case, the recombination predominantly occurs through defects in the crystal lattice and impurities that create energy levels within the bandgap. Under constant irradiation, when $\Delta n << N$ (low dose rate), the recombination rate is linearly dependent on Δn resulting in a liner dose rate response. For high dose rates ($\Delta n >> N$), other recombination mechanisms (for example, Auger and band-to-band recombination) start to play an important role (Cuevas and Macdonald, 2004) and the recombination rate is no longer proportional to Δn. Such an argument explains the nonlinearity of the dose rate response (Fig. 5), obtained under the condition that Δn is almost three orders of magnitude bigger than N. For the same reason, the dose rate responses of

the diode irradiated to 50 kGy and 100 kGy (Fig. 5) also reach saturation likewise the one assessed with the pristine diode. Another effect that also stands out in Fig. 5, is the decrease in the induced current at higher accumulated doses due to the increasing damage caused by the incoming electrons in the diode. This damage is mainly associated with the production of point defects in the crystal bulk with energy levels within the bandgap. Such defects act as recombination centers, which reduce the minority carrier lifetime and create a gradual decrease in the sensitivity. The sensitivity decay of only 9% at 100 kGy (Fig. 8), which is much smaller than those reported in the literature, validate the experimental approach of choosing a thin diode to mitigate the sensitivity loss, which is its major disadvantage when employed in a high-dose environment.

The lifespan of the diode can be predicted, considering the data presented in Fig. 8, as 75 kGy, for which the decrease in sensitivity reaches 6%. Therefore, 75 kGy is the maximum accumulated dose that the diode can withstand while still meeting the performance requirement on the response variability ($\leq$8%, k = 2) of routine dosimeters for electron beam processing according to ISO/ASTM 51649 (2015) and ISO/ASTM 51650 (2013). To maintain compliance with these regulations after accumulating 75 kGy, the diodes must be discarded and replaced with pristine samples from the same batch. However, due to the batch dose-response uniformity (3%), which is less than the experimental uncertainties of commercial EB irradiators, after their replacement, there is no need to re-calibrate the dosimetry system. It is worth noting that, although they can be reused, the low-cost (US$1.00 each) of the diodes also favors them as single-use dosimeters in radiation processing applications.

6. Conclusion

The response of thin photodiodes has been investigated in an industrial electron beam accelerator within the dose rate range of 2–8 kGy/s and accumulated doses up to 100 kGy. These devices, operating in the short-circuit mode and under industrial irradiation conditions, deliver currents nonlinearly dependent on the dose rate, whichever the dose history of the diodes, due to the high generation rates herein achieved. Despite this nonlinearity, the dose rate response is stable and characterized by current signals with repeatability better than 2.0%, regardless of the accumulated dose. Such great repeatability allows the beam dimensions, the background current, and the region corresponding to electrons scattered outside the scan window to be identified. These results reveal that the diodes might be suitable for measuring the electron beam profile and to routinely monitor the stability of the output of industrial electron accelerators. Works in this direction are currently in progress.

Moreover, the dose-response of pristine and irradiated diodes, assessed off-line by the integration of the current signals, is quite linear, at a constant dose rate, with sensitivities slightly dependent on the accumulated dose. The decrease in the charge sensitivity (9% at 100 kGy), which is much smaller than the values reported in the literature, indirectly confirms that the diode satisfies the condition of being thin even when irradiated up to 100 kGy.

Based on the latter considerations and the results presented in this work, it is possible to conclude that the diode under investigation is a low budget alternative, good enough for routine dosimetry, provided it has been previously calibrated in the same electron beam facility.

CRediT authorship contribution statement

Josemary A.C. Gonçalves: Methodology, Formal analysis, Investigation, Resources, Data curation, Funding acquisition, Project administration, Writing - review & editing. **Alessio Mangiarotti:** Methodology, Resources, Formal analysis, Writing - review & editing. **Viviane K. Asfora:** Resources, Visualization. **Helen J. Khoury:** Resources, Funding acquisition, Project administration. **Carmen C. Bueno:** Conceptualization, Methodology, Formal analysis, Writing - original draft, Writing - review & editing, Supervision.

Declaration of competing interest

The authors declare that they have no known competing financial interests or personal relationships that could have appeared to influence the work reported in this paper.

Acknowledgments

The authors highly acknowledge the collaboration of Eng. Elisabeth S. R. Somessari from the Electron Beam Accelerator staff (IPEN-CNEN/SP) for her indispensable help during the irradiations. The authors also thank R. C. Teixeira and N. Carvalho, both from Centro de Tecnologia da Informação Renato Archer (CTI-Renato Archer, Campinas/SP), for the electrical characterization of the diodes. This work is partially supported by IPEN-CNEN/SP (DPDE Edital 04/2017), FACEPE (contract nº APQ-0648-3.09/14), and CNPq (contract nº 306331/2016-0).

References

Baró, J., Sempau, J., Fernández-Varea, J.M., Salvat, F., 1995. PENELOPE: an algorithm for Monte Carlo simulation of the penetration and energy loss of electrons and positrons in matter. Nucl. Instrum. Methods B 100, 31–46. https://doi.org/10.1016/0168-583X(95)00349-5.

Barthe, J., 2001. Electronic dosimeters based on solid-state detectors. Nucl. Instrum. Methods B 184, 158–189. https://doi.org/10.1016/S0168-583X(01)00711-X.

Benedito, E., Fernández-Varea, J.M., Salvat, F., 2001. Mixed simulation of the multiple elastic scattering of electrons and positrons using partial-wave differential cross-sections. Nucl. Instrum. Methods B 174, 91–110. https://doi.org/10.1016/s0168-583x(00)00463-8.

Berger, M.J., Inokuti, M., Anderson, H.H., Bichsel, H., Dennis, J.A., Powers, D., Seltzer, S. M., Turner, J.E., 1984. Report 37: stopping powers for electrons and positrons. J. Int. Comm. Radiat. Units Meas. 19, 1984.

Berger, M.J., Jablonski, A., Bronic, I.K., Mitroy, J., Powell, C.J., Salvat, F., Sanche, L., 2007. Report 77: elastic scattering of electrons and positrons. J. Int. Comm. Radiat. Units Meas. 7, 2007.

Bruzzi, M., Bucciolini, M., Casati, M., Menichelli, D., Talamonti, C., Piemonte, C., Svensson, B.G., 2007. Epitaxial silicon devices for dosimetry applications. Appl. Phys. Lett. 90, 172109. https://doi.org/10.1063/1.2723075.

Calvo, W.A.P., Duarte, C.L., Machado, L.D.B., Manzoli, J.E., Geraldo, A.B.C., Kodama, Y., Silva, L.G.A., Pino, E.S., Somessari, E.S.R., Silveira, C.G., Rela, P.R., 2012. Electron beam accelerators - trends in radiation processing technology for industrial and environmental applications in Latin America and the Caribbean. Radiat. Phys. Chem. 81, 1276–1281. https://doi.org/10.1016/j.radphyschem.2012.02.013.

Casati, M., Bruzzi, M., Bucciolini, M., Menichelli, D., Scaringella, M., Piemonte, C., Fretwurst, E., 2005. Characterization of standard and oxygenated float zone Si diodes under radiotherapy beams. Nucl. Instrum. Methods A 552, 158–162. https://doi.org/10.1016/j.nima.2005.06.025.

Cleland, M.R., 2006. Industrial Applications of Electron Accelerators. CAS - CERN Accelerator School and KVI: Specialised CAS Course on Small Accelerators, Zeegse, The Netherlands, 24 May - 2 Jun 2005, pp. 383–416. https://doi.org/10.5170/CERN-2006-012.383 (CERN-2006-012).

Cuevas, A., Macdonalds, D., 2004. Measuring and interpreting the lifetime in silicon wafers. Sol. Energy 76, 255–262. https://doi.org/10.1016/j.solener.2003.07.033.

Damulira, E., Yusoff, M.N.S., Omar, A.F., Mohd Taib, N.H., 2019. A review: photonic devices used for dosimetry in medical radiation. Sensors 19, 2226. https://doi.org/10.3390/s19102226.

Dixon, R.L., Ekstrand, K.E., 1982. Silicon diode dosimetry. Int. J. Appl. Radiat. Isot. 33, 1171–1176.

Gilar, O., Petr, I., 1985. Silicon photodiode as a detector of exposure rate. Nucl. Instrum. Methods A 234, 566–572. https://doi.org/10.1016/0168-9002(85)91009-5.

Gildenblat, G. Sh, Goldberg, Yu, A., Levinshtein, M.E., 1996. Handbook Series on Semiconductor Parameters, vol. 1. World Scientific. Si, Ge, C (Diamond), Gaas, Gap, Gasb, Inas, Inp, Insb.

Gonçalves, J.A.C., Mangiarotti, A., Bueno, C.C., 2020. Current response stability of a commercial PIN photodiode for low dose radiation processing applications. Radiat. Phys. Chem. 167, 108276–108279. https://doi.org/10.1016/j.radphyschem.2019.04.026.

Grusell, E., Rikner, G., 1984. Radiation damage induced dose rate non-linearity in an n-type silicon detector. Acta Radiol. Oncol. 23 (6), 465–469. https://doi.org/10.3109/02841868409136050.

Hall, R.N., 1952. Electron-hole recombination in germanium. Phys. Rev. 87 (2) https://doi.org/10.1103/PhysRev.87.387, 387–387.

ICRU Report 80, 2008. International Commission on Radiation Units and Measurements, Dosimetry Systems for Use in Radiation Processing, ICRU Report 80. International Commission on Radiation Units and Measurements. https://doi.org/10.1093/jicru/ndn031, 2008.

IEC 61674, 2012. International Electrotechnical Commission, Medical Electrical Equipment - Dosimeters with Ionization Chambers And/or Semiconductor Detectors as Used in X-Ray Diagnostic Imaging, second ed. 2012.

ISO/ASTM 51649, 2015. Practice for Dosimetry in an Electron Beam Facility for Radiation Processing at Energies between 300 keV and 25 MeV, third ed. https://doi.org/10.1520/ISOASTM51649-15 2015.

ISO/ASTM 51650, 2013. Practice for Use of a Cellulose Triacetate Dosimetry System. https://doi.org/10.1520/ISOASTM51650-13, 2013.

ISO/ASTM 51707, 2015. Standard Guide for Estimation of Measurement Uncertainty in Dosimetry for Radiation Processing, third ed. https://doi.org/10.1520/ISOASTM51707-15 2015.

ISO/ASTM 52628, 2013. Standard Practice for Dosimetry in Radiation Processing, first ed. https://doi.org/10.1520/ISOASTM52628-13 2013.

JCGM 100:2008(E), GUM 1995, 2008. With minor corrections, evaluation of measurement data – guide to the expression of uncertainty in measurements. Available free of charge at the BIPM website. http://www.bipm.org.

Kitaguchi, H., Miyai, H., Izumi, S., Kaihara, A., 1996. Silicon semiconductor detectors for various nuclear radiations. IEEE Trans. Nucl. Sci. 43 (3), 1846–1850. https://doi.org/10.1109/23.507234.

Kneeland, D.R., Nablo, S.V., Weiss, D.E., Sinz, T.E., 1999. Industrial use of the real-time monitor for quality assurance in electron processing. Radiat. Phys. Chem. 55, 429–436. https://doi.org/10.1016/S0969-806X(99)00190-5.

Kuntz, F., Somessari, E.S.R., da Silveira, C.G., Bueno, C.C., Calvo, W.A.P., Napolitano, C. M., Gonçalves, J.A.C., Somessari, S.L., 2015. A dosimetric survey of the DC1500/25/04 electron beam plant installed at IPEN-CNEN/SP. In: Proceedings 2015 International Nuclear Atlantic Conference, São Paulo, Brazil, ISBN 978-85-99141-06-9.

Marre, D., Marinello, G., 2004. Comparison of p-type commercial electron diodes for in vivo dosimetry. Med. Phys. 31, 50–56. https://doi.org/10.1118/1.1630492.

Möhlmann, J.H.F., 1981. The use of solar cells for continuous recording of absorbed dose in the product during radiation sterilization. In: Biomedical Dosimetry, Proceedings of Symposium, Vienna. IAEA Publication STI/PUB/567, p. 563, 1981.

Moll, M., 2018. Displacement damage in silicon detectors for high energy physics. IEEE Trans. Nucl. Sci. 65 (8), 1561–1582. https://doi.org/10.1109/TNS.2018.2819506.

Muller, A.C., 1970a. The "n" on "p" solar-cell dose-rate meter. In: Holm, N.W., Berry, R.J. (Eds.), Manual on Radiation Dosimetry, p. 423. New York.

Muller, A.C., 1970b. The "p" on "n" solar-cell integrating dosimeter. In: Holm, N.W., Berry, R.J. (Eds.), Manual on Radiation Dosimetry, p. 429. New York.

Osvay, M., Stenger, V., Földiak, G., 1975. Silicon detectors for measurement of high exposure rate gamma rays. In: Biomedical Dosimetry, Proceedings of Symposium. IAEA Publication STI/PUB/401, Vienna, p. 623, 1974.

Osvay, M., Tárczy, K., 1975. Measurement of γ-dose rates by n- and p-type semiconductor detectors. Phys. Status Solidi 27, 285–290.

Rikner, G., Grusell, E., 1987. General specifications for silicon semiconductors for use in radiation dosimetry. Phys. Med. Biol. 32 (9), 1109–1117. https://doi.org/10.1088/0031-9155/32/9/004.

Rosenfeld, A., 2007. Electronic dosimetry in radiation therapy. Radiat. Meas. 41, S134–S153. https://doi.org/10.1016/j.radmeas.2007.01.005.

Salvat, F., 2019. PENELOPE, A Code System for Monte Carlo Simulation of Electron and Photon Transport. OECD Nuclear Energy Agency, Barcelona, Spain, 2019.

Sempau, J., Acosta, E., Baró, J., Fernández-Varea, J.M., Salvat, F., 1997. An algorithm for Monte Carlo simulation of coupled electron-photon transport. Nucl. Instrum. Methods B 132, 377–390. https://doi.org/10.1016/S0168-583X(97)00414-X.

Sempau, J., Fernández-Varea, J., Acosta, E., Salvat, F., 2003. Experimental benchmarks of the Monte Carlo code PENELOPE. Nucl. Instrum. Methods B 207, 107–123. https://doi.org/10.1016/S0168-583X(03)00453-1.

Shockley, W., Read, W.T., 1952. Statistics of the recombination of holes and electrons. Phys. Rev. 87 (5), 835–842. https://doi.org/10.1103/PhysRev.87.835.